

Cross-Consistent Deep Unfolding Network for Adaptive All-In-One Video Restoration

Yuanshuo Cheng, Mingwen Shao, *Member, IEEE*, Yecong Wan, Lixu Zhang, Wangmeng Zuo, *Senior Member, IEEE*, and Deyu Meng, *Member, IEEE*

Abstract—Existing Video Restoration (VR) methods always necessitate the individual deployment of models for each adverse weather to remove diverse adverse weather degradations, lacking the capability for adaptive processing of degradations. Such limitation amplifies the complexity and deployment costs in practical applications. To overcome this deficiency, in this paper, we propose a Cross-consistent Deep Unfolding Network (CDUN) for All-In-One VR, which enables the employment of a single model to remove diverse degradations for the first time. Specifically, the proposed CDUN accomplishes a novel iterative optimization framework, capable of restoring frames corrupted by corresponding degradations according to the degradation features given in advance. To empower the framework for eliminating diverse degradations, we devise a Sequence-wise Adaptive Degradation Estimator (SADE) to estimate degradation features for the input corrupted video. By orchestrating these two cascading procedures, CDUN achieves adaptive processing for diverse degradation. In addition, we introduce a window-based inter-frame fusion strategy to utilize information from more adjacent frames. This strategy involves the progressive stacking of temporal windows in multiple iterations, effectively enlarging the temporal receptive field and enabling each frame’s restoration to leverage information from distant frames. Extensive experiments demonstrate that the proposed method achieves state-of-the-art performance in All-In-One VR.

Index Terms—Deep learning, All-In-One Video Restoration, Deep Unfolding Network, Convolutional Neural Network, Transformer.

I. INTRODUCTION

VIDEOS captured in the real world often suffer from quality reduction due to adverse weather degradations such as rain, haze, snow, and low light. Consequently, the performances of subsequent downstream tasks such as object detection [1], [2] and segmentation [3], [4] will be significantly impaired. In order to restore clean backgrounds from frames corrupted by degenerations, a number of Video Restoration (VR) methods have been proposed to utilize complementary redundancy information in adjacent frames to restore the damaged content. These methods can be categorized into explicit [5]–[7] and implicit paradigms [8], [9]. Explicit methods generally perform frame alignment among several adjacent frames based on optical flow [10] or deformable convolution [11], which subsequently fuses background features from multiple frames in an aligned feature space. Implicit methods, on the other hand, train an end-to-end neural network to directly mine helpful information from unaligned adjacent frames. However, existing video restoration methods all follow a “Task-Specific”

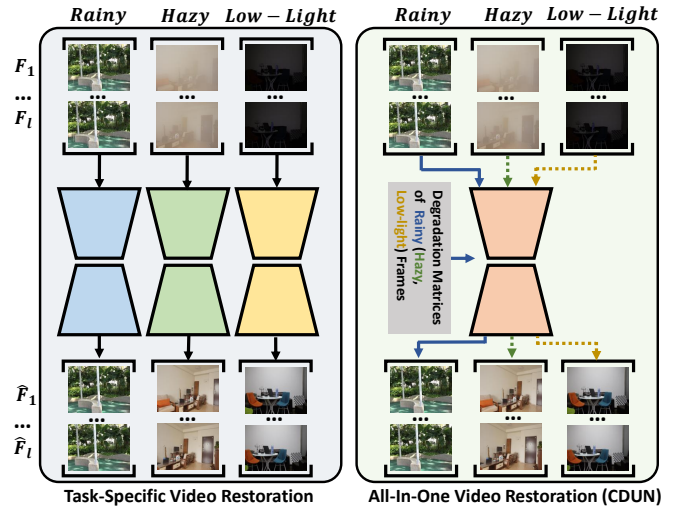


Fig. 1. Task-Specific VR require designing and training separate models for each type of degradation. The proposed CDUN achieves adaptive handling of different degradation types by adaptively adjusting degradation matrices, leading to the first-ever realization of an All-In-One VR.

paradigm, which means that a single model can only remove one specific type of degradation and cannot adaptively handle different degradations with a unified model. In real-world scenarios with diverse degradations, existing methods necessitate training and deploying models separately for each degradation type, which results in exorbitant application costs. Therefore, repairing videos corrupted by different degradations using a unified model (All-In-One VR) is a pressing issue.

Most recently, several efforts have been made to learn to remove diverse unknown degradations from corrupted images using a single model [12]–[16]. Although these methods achieve promising performances in Image Restoration (IR), they suffer from severe limitations in processing video data caused by their inability to exploit complementary redundant features among adjacent frames. Therefore, the All-In-One VR involves not only 1) enabling a single model to autonomously adapt to different degradation removal tasks, but also 2) realizing the extraction of complementary background information from multiple adjacent frames to improve the quality of the restored frames.

The Deep Unfolding Network (DUN) [17]–[19] is a feasible paradigm to deal with the above challenges. Firstly, the DUNs can restore images corrupted by diverse degradations according to the pre-given features of different degradations [20]. Secondly, the DUNs can enable extracting complementary features by modeling the correspondences among adjacent

Yuanshuo Cheng, Mingwen Shao and Yecong Wan are with the College of Computer Science and Technology, China University of Petroleum, China.

frames [21]. Nevertheless, such methods require providing features of each degradation in advance and are unable to adaptively generate them when dealing with different degradations. Therefore, they do not allow for the unified removal of diverse degradations. Besides, existing methods can only model frames within a short temporal window, which leads to a narrow temporal receptive field. This shortcoming limits the capturing of useful information from a longer temporal-range of frames.

To address the aforementioned issues, in this paper, we proposed a DUN-based All-In-One VR framework (as shown in Fig. 1.), called Cross-Consistent Deep Unfolding Network (CDUN), to remove diverse adverse weather degradations in videos with a single model. CDUN implements adaptive estimation for unknown degradation features to guide the model to remove diverse degradations. And meanwhile, it effectively utilizes the temporal complementary information from long temporal-range frames.

Specifically, we propose a novel Sequence-wise Adaptive Degradation Estimator (SADE) to adaptively estimate the features of unknown degradation in the input video. According to the estimated degradation features, we construct an iterative optimization framework based on Maximum A Posteriori (MAP) to solve for the clean background corrupted by this degradation. With the above two cascading procedures, the proposed method can realize autonomous adaptation for diverse degradation removal tasks. In addition, we propose a Cross-Consistency strategy to align the background features of the frames in the same temporal window. This strategy enables the restoration of each frame to obtain helpful information from multiple frames in the same temporal window. More importantly, the progressively iterative architecture of CDUN leads to the stacking of multiple temporal windows, thereby expanding the temporal receptive field. Thus, after multi-step iterative optimization, the proposed method can capture background information from frames at a greater distance rather than being limited to within only one temporal window.

In summary, the main contributions of this work are as follows:

- In this paper, we propose an All-In-One VR framework called CDUN for the first time, which enables the unified removal of diverse adverse weather degradations from videos employing a single model. Extensive experiments demonstrate that the proposed CDUN outperforms existing methods.
- We propose a novel SADE to estimate features of unknown degradations in the input videos, which subsequently guides an optimization framework to handle diverse degradation removal tasks according to the estimated features.
- A stacked-window-based background feature fusion strategy is devised in this paper, which utilizes the iterative architecture to progressively expand the temporal receptive field. This enables the capturing and utilization of complementary background information from a long temporal-range of frames.

(Note: In this paper, (1) unless otherwise specified, all multiplication operations refer to element-wise multiplication

(Hadamard product); (2) all operations involving a single scalar and a matrix are equivalent to performing the operation on each element of the matrix with the scalar); (3) in the context of an image / frame, the portion other than the degradation is referred to as the "background".

II. RELATED WORK

A. Video Restoration

The VR task is dedicated to mining complementary background information from adjacent frames to restore the corrupted backgrounds. Most of the early works explicitly aligns adjacent frames based on the estimated optical flows [10], [22], [23] or the offsets of the deformable convolutions [11], [24], which consequently enables the sharing and utilization of complementary features among these frames. Nevertheless, the accuracy of explicit alignment is susceptible to long displacements [25] and motion blur [26]. Therefore, some subsequent works propose more robust implicit methods to utilize complementary features directly. For instance, Zhu *et al.* [8] cancel the frame alignment procedure and focus solely on fusing features from unaligned adjacent frames via an well-designed neural network. In addition, limited by the computational cost, these methods are mostly constructed based on sliding window [25], [27], [28] or recurrent architectures [29]–[31]. Both of these architectures have a short temporal receptive field and are unable to utilize the information from more distant frames. To address this issue, Liang *et al.* [32] propose a model that incorporates Temporal Mutual Self Attention and Parallel Warping to achieve long-range modeling capability. Although existing efforts have made promising progress in VR, a single model in these methods can only deal with one type of degradation. Therefore, the deployment of multiple models is required to cater to multi-degradation scenarios, which bear a high application cost. In contrast, our method is able to adaptively restore videos corrupted by diverse degradations with a single model.

B. All-in-one Image Restoration

Most recently, several efforts attempt to develop All-In-One IR [12], [13], [33]–[35] frameworks to restore images corrupted by different degradations with a single model. The key to All-In-One IR lies in developing effective techniques to adapt a single model to different degradation types. To this end, Li *et al.* [12] devise a model with multiple encoders to remove multiple degradations, which is the first successful implementation of All-In-One IR. However, in order to choose the corresponding encoder, this approach requires providing the degradation type in advance, which hinders the implementation of an end-to-end framework. Therefore, some further works tend to develop more convenient frameworks to enable the model to autonomously discriminate the degradation type and remove the corresponding degradations. For instance, Chen *et al.* [14] propose using knowledge distillation to enable an All-In-One student model to learn the removal capabilities of diverse degradations from multiple Task-Specific teacher models. Zhu *et al.* further discover that different weather

degradations exhibit specific and general features, and suggest enhancing the multi-degradation removal capability by learning these two features. Compared to these All-In-One IR methods, our proposed All-In-One VR framework not only can adaptively remove diverse degradations, but also utilizes the abundant complementary features in multiple frames to improve the quality of the restored frames.

C. Deep Unfolding Network

The IR task can be formulated as a MAP problem, which can be solved by minimizing the established energy function. To this end, some works introduce deep neural networks (DNNs) into traditional optimization algorithms to develop efficient solving methods, which is the fundamental paradigm of DUNs. Specifically, the deep unfolding methods unfold the energy function into a fidelity term-related subproblem and a regular term-related subproblem [40], [41], and minimize the energy function by alternately optimizing the two subproblems. The earlier works employ handcrafted prior constraints [42], [43] to optimize the regular term-related subproblems, but they typically suffer from cumbersome crafting processes and a limited representation ability. To overcome this drawback, Zhang *et al.* [17] firstly propose to use DNN prior to replace the hand-crafted prior, which simplifies the algorithmic process through end-to-end training. Meanwhile, DNNs can fit complex priors in a data-driven manner, which enables DUNs to effectively handle more challenging degradations such as low light [19], shadow [44], rain [18], etc. In addition, the degradation model in the fidelity term determines the type of degradation that the DUNs can handle. Therefore, the DUNs can be adapted to different IR tasks by utilizing different degradation models. Leveraging this capability, Zhang *et al.* [20] devised a DUN-based method that achieves unified image super-resolution with different noise levels and blur kernels. However, since the degradation features (i.e., noise and blur kernels) need to be given manually, this approach cannot implement an end-to-end framework. Unlike the aforementioned works, our method can flexibly restore videos corrupted by different degradations by adaptively adjusting the degradation model.

III. METHODOLOGY

In this section, we first introduced the proposed Cross-Consistency, which serves as the foundation for constructing CDUN. Based on Cross-Consistency, we provided the formalized representation of CDUN. Then, we presented the unfolding-based optimization strategy. Subsequently, we described the overall framework and training process of CDUN. Finally, we explained the structure and roles of the crucial modules.

A. Cross-Consistency

Cross-Consistency serves as the foundation for the proposed CDUN. It models the relationship between degraded frames, degradation matrices, and clean frames within a temporal window.

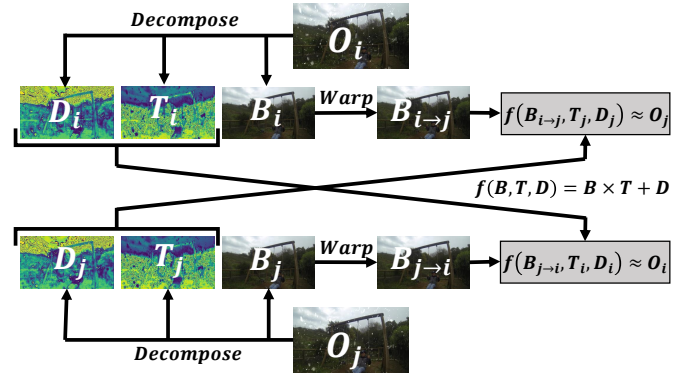


Fig. 2. Framework of Cross-Consistency. Cross-Consistency can be summarized as: For two adjacent frames (F_i, F_j), apply a motion operation to their background and exchange the degradation matrices. Consequently, they should transform into each other (F_j, F_i).

We observed that most degradation types, such as rain [45], haze [46], snow [47], and low-light [48], can be modeled by an additive factor and a multiplicative factor [49]:

$$F_i = T_i \cdot B_i + D_i, \quad (1)$$

where T_i and D_i are collectively referred to as degradation matrices. F_i represents the i -th frame in the frame sequence, and B_i corresponds to the clean background associated with F_i , which is our desired target for restoration. For two adjacent degraded frames' clean backgrounds, B_i and B_j , the pixels in them exhibit a certain motion relationship, which can be represented as $M_{i \to j}(B_i) \approx B_j$. $M_{i \to j}(\ast)$ is a motion operator introduced to perform motion on the image \ast based on the correspondence of the movements (optical flow) from B_i to B_j (see Sec. III-F for implementation details). In this case, when we apply the degradation matrix of F_j (i.e. T_j and D_j) to $M_{i \to j}(B_i)$, the resulting image should be approximately equal to F_j . Therefore, Cross-Consistency can be formulated as follows:

$$E_{B_i}[M_{i \to j}(B_i) \cdot T_j + D_j] = F_j, \quad (2)$$

where E denotes the mathematical expectation. Additionally, Fig. 2 further visualizes the principles of Cross-Consistency.

B. Problem Formulation

Unlike IR, VR requires gathering information from adjacent frames to aid in the restoration process. Therefore, the MAP framework for video restoration can be represented as follows:

$$\begin{aligned} \hat{B}_i &= \arg \max_{B_i} \sum_{j \in \mathcal{I}} \log P(B_i | F_j) \\ &= \arg \min_{B_i} \left[\frac{1}{2n+1} \sum_{j \in \mathcal{I}} \log P(F_j | B_i) + \log P(B_i) \right], \end{aligned} \quad (3)$$

where \mathcal{I} represents a temporal window, and $\mathcal{I} = \{i-n, \dots, i-1, i, i+1, \dots, i+n\}$. In practice, n is set to 1, meaning that \mathcal{I} is a window of length 3. Based on the Cross-Consistency

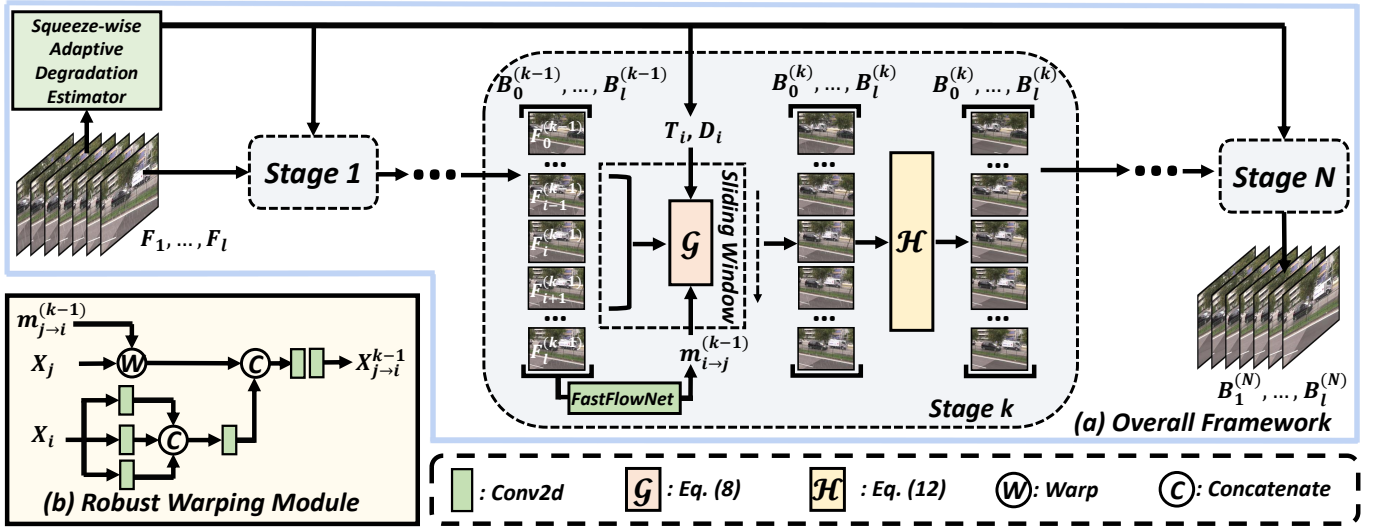


Fig. 3. Illustration of Cross-Consistent Deep Unfolding Network (CDUN). (a) Overall framework of CDUN. The proposed CDUN achieves All-In-One VR for the first time. CDUN addresses the challenges of adaptive handling of multiple degradations in VR and the enlargement of temporal receptive fields.(b) The structure of Robust Warping Module (RWM). RWM implements explicit pixel motion based on optical flow and demonstrates low motion errors.

principle, we represent the All-In-One VR as a problem of minimizing the following energy function:

$$\hat{B}_i = \arg \min_{B_i} \frac{1}{2n+1} \sum_{j \in \mathcal{I}} \frac{1}{2} \|W_{i \rightarrow j} \{F_j - [M_{i \rightarrow j}(B_i) \cdot T_j + D_j]\}\|^2 + \lambda \Phi(B_i), \quad (4)$$

where $W_{i \rightarrow j}$ represents spatial motion weight, which is dependent on the motion distances of individual pixels. $W_{i \rightarrow j}$ can alleviate the issue of motion error interference during the restoration process. λ is a trade-off parameter.

As the degradation matrices T_j and D_j define the type and features of degradation that this algorithm aims to address, the flexible handling of multiple degradations can be achieved by adaptively setting T_j and D_j accordingly. Here we summarize how the CDUN achieves adaptive handling of different degradations as : (1) Decoupling and modeling the relationships between degradation matrices, degraded frames, and clean frames, through Cross-Consistency; (2) adaptively estimating the degradation matrices of degraded frames to enable the model to handle corresponding types of degradations.

C. Unfolding Optimization

By employing the Half Quadratic Splitting (HQS) algorithm [40], Eq. 4 can be unfolded into two sub-problems: one related to the fidelity term and the other related to the regularization term. The optimization of Eq. 4 can then be achieved by iteratively optimizing these two sub-problems alternately. The degradation matrices operate during the solution process of the fidelity term-related sub-problem. By adaptively estimating the degradation matrices, CDUN achieves control over the types of degradation being addressed. The optimization of the regularization term-related sub-problem is achieved by introducing a CNN prior. Compared to traditional Gaussian denoising priors [17], [50], the CNN prior offers the advantages of stronger robustness and convenience of acquisition through end-to-end

training. Specifically, by introducing an auxiliary variable Z , Eq. 4 can be rewritten as follows:

$$\hat{B}_i = \arg \min_{B_i} \frac{1}{2n+1} \sum_{j \in \mathcal{I}} \frac{1}{2} \|W_{i \rightarrow j} \{F_j - [M_{i \rightarrow j}(Z_i) \cdot T_j + D_j]\}\|^2 + \lambda \Phi(B_i) \text{ s.t. } Z_i = B_i. \quad (5)$$

To handle the equality constraint in the above equation, we introduce a quadratic term and rewrite the equation in an unconstrained form:

$$\hat{B}_i = \arg \min_{B_i} \frac{1}{2n+1} \sum_{j \in \mathcal{I}} \frac{1}{2} \|W_{i \rightarrow j} \{F_j - [M_{i \rightarrow j}(Z_i) \cdot T_j + D_j]\}\|^2 + \frac{\gamma}{2} \|Z_i - B_i\|^2 + \lambda \Phi(B_i), \quad (6)$$

where γ is a penalty parameter. According to the HQS algorithm [40], Eq. 6 can be decomposed into two sub-problems and optimized alternately:

$$\hat{Z}_i = \arg \min_{Z_i} \frac{1}{2n+1} \sum_{j \in \mathcal{I}} \frac{1}{2} \|W_{i \rightarrow j} \{F_j - [M_{i \rightarrow j}(Z_i) \cdot T_j + D_j]\}\|^2 + \frac{\gamma}{2} \|Z_i - B_i\|^2, \quad (7a)$$

$$\hat{B}_i = \arg \min_{B_i} \frac{\gamma}{2} \|Z_i - B_i\|^2 + \lambda \Phi(B_i). \quad (7b)$$

Eq. 7a is a least-squares problem, and we can directly calculate its closed-form solution:

$$\hat{Z}_i = \frac{\gamma B_i + \sum_{j \in \mathcal{I}} U_{i \rightarrow j} M_{j \rightarrow i} [T_j (F_j - D_j)] / (2n+1)}{\sum_{j \in \mathcal{I}} U_{i \rightarrow j} M_{j \rightarrow i} (T_j^2) / (2n+1) + \gamma}, \quad (8)$$

where $U_{i \rightarrow j} = M_{j \rightarrow i} (W_{i \rightarrow j}^2)$. In practice, we directly compute $U_{i \rightarrow j}$ instead of $W_{i \rightarrow j}$. The reason and related analysis is detailed in Sec. III-G. During the solution process, T_j and D_j are estimated using the proposed SADE, and the specific details can be found in Sec. III-E. The motion operator $M_{j \rightarrow i}$ is implemented through the proposed RWM, and the detailed implementation method is presented in Sec. III-F. $U_{i \rightarrow j}$ is

related to the motion distances from B_i to B_j , and the detailed calculation method is elaborated in Sec. III-G.

Here, we clarify some critical details during the derivation process of Eq. 8. Firstly, we construct the following function according to Eq. 7a:

$$L(Z_i) = \frac{1}{2n+1} \sum_{j \in \mathcal{I}} \frac{1}{2} \|W_{i \rightarrow j} \{F_j - [M_{i \rightarrow j}(Z_i) \cdot T_j + D_j]\}\|^2 + \frac{\gamma}{2} \|Z_i - B_i\|^2. \quad (9)$$

The result of Eq. 8 can be obtained by letting $\frac{\partial L}{\partial Z_i} = 0$. For the differentiation of the $M_{i \rightarrow j}$, we can deduce it by induction from the differentiation of the matrix transpose. For matrix transpose, we have $\frac{\partial X^T}{\partial X} = C$, where C is a commutation matrix. Since both $M_{i \rightarrow j}$ and matrix transpose operations alter the positions of elements in a matrix, we can assert that $\frac{\partial M_{i \rightarrow j}(X)}{\partial X} = C'$. Here, C' represents a presumed generalized commutation matrix. Consequently, we have:

$$A \frac{\partial M_{i \rightarrow j}(X)}{\partial X} = \text{mat}(\text{vec}(A) \times C') = M_{i \rightarrow j}^{-1}(A), \quad (10)$$

where \times denotes matrix multiplication. vec denotes the operation of flattening matrix elements into a row vector, and mat represents the operation of reconstructing the row vector back into a matrix. A is a matrix of the same size as X , and \cdot represents element-wise multiplication (Hadamard product). $M_{i \rightarrow j}^{-1}(\cdot)$ represents the inverse operation of $M_{i \rightarrow j}(\cdot)$, which involves moving the variable \cdot based on the motion relationship (optical flow) from B_j to B_i . Additionally, the motion operator $M_{i \rightarrow j}$ possesses several properties that are utilized during the derivation process:

$$M_{i \rightarrow j}^{-1}(A) = M_{j \rightarrow i}(A), \quad (11a)$$

$$M_{i \rightarrow j}^{-1}(M_{i \rightarrow j}(A)) = A, \quad (11b)$$

$$M_{i \rightarrow j}(A + B) = M_{i \rightarrow j}(A) + M_{i \rightarrow j}(B), \quad (11c)$$

$$M_{i \rightarrow j}(A + c) = M_{i \rightarrow j}(A) + c, \quad (11d)$$

$$M_{i \rightarrow j}(AB) = M_{i \rightarrow j}(A)M_{i \rightarrow j}(B), \quad (11e)$$

$$M_{i \rightarrow j}(cA) = cM_{i \rightarrow j}(A). \quad (11f)$$

where A and B are two matrices of the same size. c is a scalar.

For the optimization of the regularization term-related subproblem (*i.e.* Eq. 7b), we trained a CNN model based on the U-Net [51] architecture to approximate the implicit prior. This process can be formulated as follows:

$$\hat{B}_i = U\text{Net}(Z_i). \quad (12)$$

Compared to manually crafted priors, priors fitted through data-driven learning methods possess stronger robustness. Moreover, the end-to-end training process is more straightforward than manual design. In practice, the parameters of the U-Net are not shared across different iterations.

D. Overall Framework and Training Process for Cross-Consistent Deep Unfolding Network

Fig. 3(a) illustrates the overall framework of CDUN. First, we utilize SADE to estimate the degradation matrices (see Sec. III-E) of the given degraded frames $\mathcal{V} = \{F_i \in \mathbb{R}^{3 \times H \times W} | i =$

Algorithm 1 Cross-Consistent Deep Unfolding Network

```

1: Input:  $\mathcal{V} = \{F_i \in \mathbb{R}^{3 \times H \times W} | i = 1, 2, \dots, l\}$ 
   /* degraded video of length  $l$  */
2: Output:  $\mathcal{B}^{(N)} = \{B_i^{(N)} \in \mathbb{R}^{3 \times H \times W} | i = 1, 2, \dots, l\}$ 
   /* clean video of length  $l$  */
3:  $\{T_i, D_i \in \mathbb{R}^{1 \times H \times W} | i = 1, 2, \dots, l\} = \text{SADE}(\mathcal{V})$ 
   /* estimate degradation matrix with Eq. 16b */
4:  $\mathcal{B}^{(0)} = \{B_i^{(0)} | B_i^{(0)} = F_i, i = 1, 2, \dots, l\}$ 
5:  $\gamma^0 = 0.1$ 
6:  $s = 0.05$  /* initialize  $\mathcal{B}^{(0)}$ ,  $\gamma^{(0)}$  and  $s$  */
7: for  $k = 1 \rightarrow N$ : /*  $N$  iterations */
8:   for  $i = 1 \rightarrow l$ :
9:     if  $i = 1$ :
10:       $\mathcal{I} = \{2, 1, 3\}$ 
11:     else if  $i = l$ :
12:       $\mathcal{I} = \{l - 2, l, l - 1\}$ 
13:     else:
14:       $\mathcal{I} = \{i - 1, i, i + 1\}$  /* temporal window */
15:     end if
16:     for  $j$  in  $\mathcal{I}$ :
17:       $m_{i \rightarrow j}^{(k-1)} \in \mathbb{R}^{2 \times H \times W} = \text{FastFlowNet}(F_i^{(k-1)}, F_j^{(k-1)})$  /* optical flow */
18:       $M_{i \rightarrow j}^{(k-1)}(\cdot) = \text{RWM}(\cdot, m_{i \rightarrow j}^{(k-1)})$  /* Eq. 19a and 19b */
19:       $U_{i \rightarrow j}^{(k-1)} \in \mathbb{R}^{1 \times H \times W} = \mathcal{F}(\|m_{i \rightarrow j}^{(k-1)}\|^2)$  /* Eq. 23 */
20:     end for
21:      $Z_i^{(k)} = \frac{\gamma B_i^{(k-1)} + \sum_{j \in \mathcal{I}} U_{i \rightarrow j}^{(k-1)} M_{j \rightarrow i}^{(k-1)} [T_j (F_j - D_j)]}{\sum_{j \in \mathcal{I}} U_{i \rightarrow j}^{(k-1)} M_{j \rightarrow i}^{(k-1)} (T_j^2) / (2n+1) + \gamma^{(k-1)}}$  /* Eq. 8 */
22:      $B_i^{(k)} = U\text{Net}(Z_i^{(k)})$  /* Eq. 12 */
23:   end for
24:    $\mathcal{B}^{(k)} = \{B_i^{(k)} | i = 1, 2, \dots, l\}$ 
25:    $\gamma^{(k)} = \gamma^{(k-1)} + s$ 
26: end for
27: Return  $\mathcal{B}^{(N)}$ 

```

$1, 2, \dots, l\}$. Subsequently, we solve for the clean frames by iteratively optimizing Eq. 4. Since the motion operator $M_{i \rightarrow j}$ (see Sec. III-F) and the spatial motion weight (see Sec. III-G) are both based on optical flow, at the beginning of each iteration stage, we first estimate the optical flow between adjacent frames using FastFlowNet [52]. Then, we iteratively execute Eq. 8 and Eq. 12 alternately to optimize Eq. 4. Similar to existing methods [19], [20], the penalty parameters γ increases during the iterative process. The output sequence $\mathcal{B}^{(N)} = \{B_i^{(N)} \in \mathbb{R}^{3 \times H \times W} | i = 1, 2, \dots, l\}$, obtained after N iterations, represents the video restoration result. We present the detailed pseudocode for the inference process of CDUN in Algorithm 1. Indeed, Eq. 8 involves a sliding window process. Multiple iterations achieve the stacking of windows, thereby expanding the temporal receptive field. Moreover, since the corresponding degradation can be removed by optimizing Eq. 4 when the degradation matrices is known, CDUN achieves All-In-One video restoration by employing SADE to estimate the degradation matrix in an All-In-One manner.

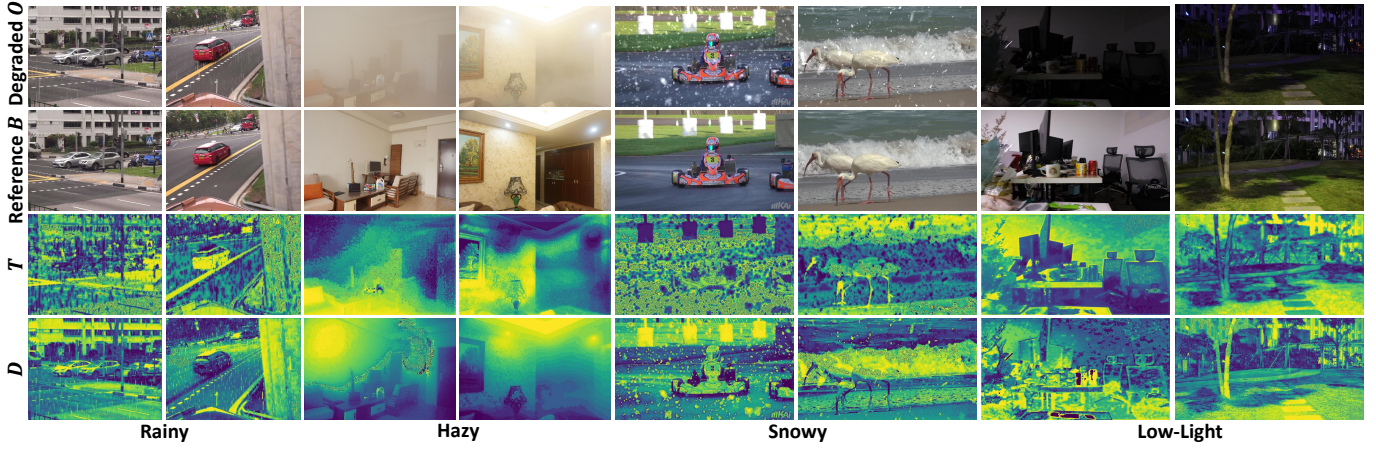


Fig. 4. The visualization displays the degradation matrices. The proposed SADE adaptively predicts the degradation matrices T and D model the degradation category and features. This serves as one of the key factors guiding the proposed CDUN’s adaptive handling of different degradations. It is worth noting that although the general degradation process includes a multiplicative factor and an additive factor (see Eq. 1), it merely aims to encompass various forms of degradation modeling. In practice, T lacks practical significance in rain modeling, while D lacks practical significance in low-light modeling.

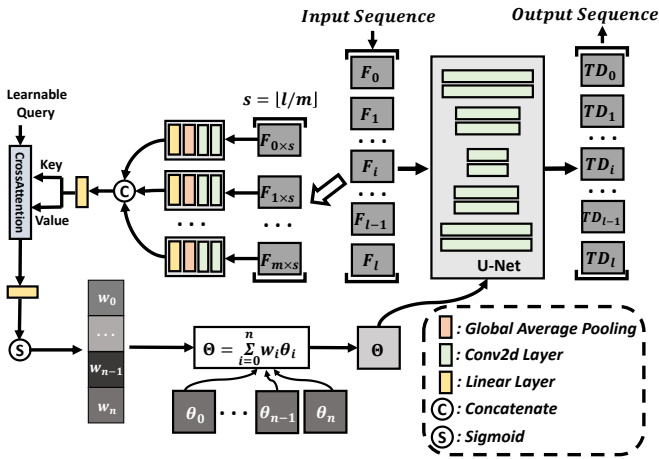


Fig. 5. Structure of Sequence-wise Adaptive Degradation Estimator (SADE). This work achieves adaptive processing for different degradation types based on adaptively estimating the degradation matrices using SADE.

The proposed method consists of a two-stage training process. In the first stage, we initially train an SADE, and its details along with the loss function can be found in Sec III-E. Additionally, the weights of FastFlowNet [52] are provided by the official source and do not require additional training. Afterwards, we freeze the parameters of SADE and FastFlowNet and train CDUN in an end-to-end manner. The loss function \mathcal{L}_{CDUN} consists of SSIM loss [53] and Charbonnier loss [54] and can be represented as follows:

$$\mathcal{L}_{sup}(x, y) = [1 - SSIM(x, y)] + \sqrt{\|x - y\|^2 + \epsilon^2}, \quad (13a)$$

$$\mathcal{L}_{CDUN}(\mathcal{B}^{(N)}, \mathcal{Y}) = \frac{1}{l} \sum_{i=1}^l \mathcal{L}_{sup}(B_i^{(N)}, Y_i), \quad (13b)$$

where $\epsilon = 0.001$. $\mathcal{Y} = \{Y_i \in \mathbb{R}^{3 \times H \times W} | i = 1, 2, \dots, l\}$ represents the paired grand-truth video.

E. Sequence-wise Adaptive Degradation Estimator

Dynamic networks can adjust network parameters [55], [56] or structures [57], [58] flexibly based on the input to

handle different degradation types. Taking dynamic parameters as an example [59], existing methods often generate a set of parameters based on the input image’s features and then process that image (referred to as image-wise dynamic or frame-wise dynamic). Since the degradation type is generally consistent within the same frame sequence, and our objective is to dynamically extract degradation features, we consider that sharing the same set of parameters among frames in the sequence is sufficient to meet the requirements (referred to as sequence-wise dynamic). The classical frame-wise dynamic approach not only wastes computational resources but also exhibits instability compared to the sequence-wise dynamic approach (as discussed in Sec. IV-D). The proposed sequence-wise dynamic method addresses this by observing multiple frames to generate parameters, achieving dynamic parameters across sequences and shared parameters within a sequence.

Specifically, as shown in Fig 5, for the input sequence $\mathcal{V} = \{F_i \in \mathbb{R}^{3 \times H \times W} | i = 1, 2, \dots, l\}$, we extract sequence features to generate weights. To reduce computational complexity, we perform equidistant sampling of $m = 5$ frames instead of using all frames, with a sampling interval of $\lfloor l/m \rfloor$ ($\lfloor * \rfloor$ represents round down). Afterward, we utilize convolution, global average pooling, and linear mapping to extract degradation features from multiple sample frames as the degradation feature set $\mathcal{P} = \{p_i \in \mathbb{R}^{1 \times C} | i = 1, 2, \dots, m\}$ for the video \mathcal{V} . C represents the number of channels. We then concatenate all the feature vectors to obtain $P \in \mathbb{R}^{C \times m \times 1}$. We utilize learnable queries $Q \in \mathbb{R}^{C \times n \times 1}$ and cross-attention [60] to explore the information from each feature vector and combine them into a fixed-size feature vector. We then generate expert weights $W \in \mathbb{R}^{n \times 1}$ through a sigmoid function. The aforementioned process can be formulated as follows:

$$W = \text{Sigmoid}\{L[\text{Softmax}(\frac{L(Q)L(P)^T}{\sigma})L(P)]\}, \quad (14)$$

where $L(*)$ represents the linear layer. With this expert weight, we combine n experts (learnable parameter θ_i):

$$\Theta = \sum_{i=0}^n w_i \theta_i, \quad (15)$$

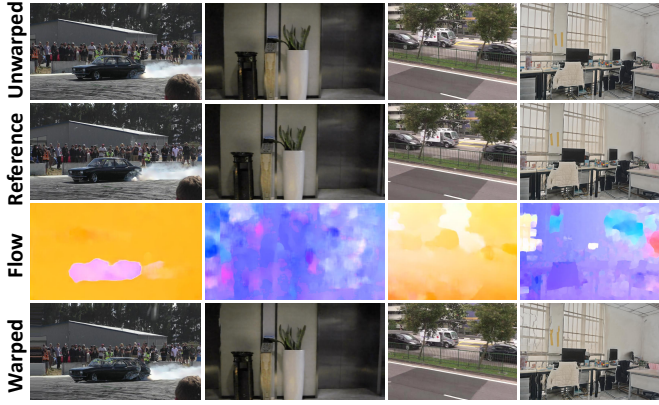


Fig. 6. Explicit optical flow-based warping operation may lead to structural errors. As shown in the figure, we applied warping operations to images using the optical flow estimated by FastFlowNet [52]. It can be observed that the structural distortion is evident in the warped image. The proposed RWM alleviates this issue by incorporating the structural information of the target image during warping operations.

where w_i is a component of W . Since this work involves All-In-One VR experiments for 4 types of degradations, using four sets of dynamic parameters (*i.e.*, $n = 4$) is sufficient. The obtained dynamic parameter Θ is used as the parameter for the U-Net, and the degradation matrices ($\mathcal{T} = \{T_i \in \mathbb{R}^{1 \times H \times W} | i = 1, 2, \dots, l\}$ and $\mathcal{D} = \{D_i \in \mathbb{R}^{1 \times H \times W} | i = 1, 2, \dots, l\}$) for the frame sequence $\mathcal{V} = \{F_i \in \mathbb{R}^{3 \times H \times W} | i = 1, 2, \dots, l\}$ will be estimated:

$$T_i, D_i = \text{split}[\text{UNet}(F_i; \Theta)], \quad (16a)$$

$$\mathcal{T}, \mathcal{D} = \text{SADE}(\mathcal{V}), \quad (16b)$$

where *split* indicates the operation of splitting along the channel dimension. SADE follows an end-to-end supervised training approach, and its loss function \mathcal{L}_{SADE} is defined as:

$$\mathcal{L}_{SADE}(\mathcal{T}, \mathcal{D}, \mathcal{V}, \mathcal{Y}) = \sum_{i=1}^l \mathcal{L}_{sup}[(F_i - D_i)/T_i, Y_i], \quad (17)$$

where $\mathcal{Y} = \{Y_i \in \mathbb{R}^{3 \times H \times W} | i = 1, 2, \dots, l\}$ represents the ground-truth video, and \mathcal{L}_{sup} has been defined in Eq. 13a.

F. Robust Warping Module

In VR, frame alignment is crucial for utilizing information from adjacent frames. Existing explicit alignment methods [22]–[24] are susceptible to large displacements or motion blur, which can negatively impact their precision. To avoid this shortcomings, some recent researches open employ implicit alignment methods [21], [61]. However, this work relies on the explicit $M_{i \rightarrow j}$ operator and cannot utilize implicit methods. To address the mentioned issue, we propose a Robust Warping Module (RWM) to implement the $M_{i \rightarrow j}$ operator. The RWM retains the explicit alignment paradigm while overcoming the precision limitations of explicit methods.

The detailed structure of the Robust Warping Module (RWM) is illustrated in Fig. 3(b). Specifically, we correct potential structural errors (as shown in Fig. 6) in the warped matrix by incorporating structural information from the target matrix during the warping process. From Eq. 8, it is clear

that $M_{j \rightarrow i}$ directly operates on matrices $T_j(F_j - D_j)$ and T_j^2 . Taking the former as an example, we first apply the $\text{Warp}_{j \rightarrow i}$ operation to matrix $T_j(F_j - D_j)$ based on the optical flow $m_{j \rightarrow i}$. According to Eq. 1, the spatial structure of $M_{j \rightarrow i}[T_j(F_j - D_j)]$ should be similar to $T_i(F_i - D_i)$ (target matrix). Therefore, we propose to utilize $T_i(F_i - D_i)$ to correct structural errors in $\text{Warp}_{j \rightarrow i}[T_j(F_j - D_j)]$. We extract the structural information from $T_i(F_i - D_i)$ using three convolutional layers (3×3 , 5×5 and 5×5 with *dilation* = 2) with different receptive field sizes. Subsequently, we concatenate this structural information with $\text{Warp}_{j \rightarrow i}[T_j(F_j - D_j)]$. And finally, two additional convolutional layers is used to fuse the information. The execution process of RWM can be formulated as follows (corresponding to Fig. 3(b)):

$$\text{RWM}(X_j, X_i, m_{j \rightarrow i}) = \text{Conv}_{\times 2}\{\text{Cat}[\text{Warp}(X_j, m_{j \rightarrow i}), S(X_i)]\}, \quad (18a)$$

$$S(X_i) = \text{Conv}\{\text{Cat}[\text{Conv}_{3 \times 3}(X_i), \text{Conv}_{5 \times 5}(X_i), \text{Conv}_{5 \times 5, \text{dilation}=2}(X_i)]\}, \quad (18b)$$

where X_j represents the matrix to be warped, X_i denotes the target matrix. *Conv* denotes the convolutional layer, and *Cat* signifies concatenating. *Warp* denotes the process of displacing individual pixels based on the optical flow. Correspondingly, $M_{j \rightarrow i}^{(k-1)}[T_j(F_j - D_j)]$ and $M_{j \rightarrow i}^{(k-1)}(T_j^2)$ in Algorithm 1 can be represented as:

$$M_{j \rightarrow i}^{(k-1)}[T_j(F_j - D_j)] = \text{RWM}[T_j(F_j - D_j), T_i(F_i - D_i), m_{j \rightarrow i}^{(k-1)}], \quad (19a)$$

$$M_{j \rightarrow i}^{(k-1)}(T_j^2) = \text{RWM}(T_j^2, T_i^2, m_{j \rightarrow i}^{(k-1)}). \quad (19b)$$

G. Spatial Motion Weight

Generally, in the process of frame alignment, long-distance motion often exhibit larger errors compared to short-distance displacements. Hence, pixels that have moved different distances in adjacent frames contribute differently to the restoration of the current frame. In order to mitigate the impact of motion errors on the fusion of adjacent frame information, we allocate weights (*i.e.* $W_{i \rightarrow j}$ in Eq. 4) to each pixel based on the distance it has moved.

Specifically, the optical flow map consists of two channels, representing the horizontal and vertical distances moved by each pixel. Therefore, we can directly calculate the movement distances of individual pixels by $\sqrt{\|m_{i \rightarrow j}\|^2}$. In practice, we use $\|m_{i \rightarrow j}\|^2$ instead of $\sqrt{\|m_{i \rightarrow j}\|^2}$, which can also serve as a distance metric and avoid the additional computational complexity of square root calculations. In the matrix after movement, the distance moved by a certain pixel to reach its current position can be represented as $M_{i \rightarrow j}(\|m_{i \rightarrow j}\|^2)$. Afterward, we employ a trainable weight generation network, denoted as f , to generate weights based on the distances of movement. This can be represented as follows:

$$W_{i \rightarrow j} = f[M_{i \rightarrow j}(\|m_{i \rightarrow j}\|^2)]. \quad (20)$$

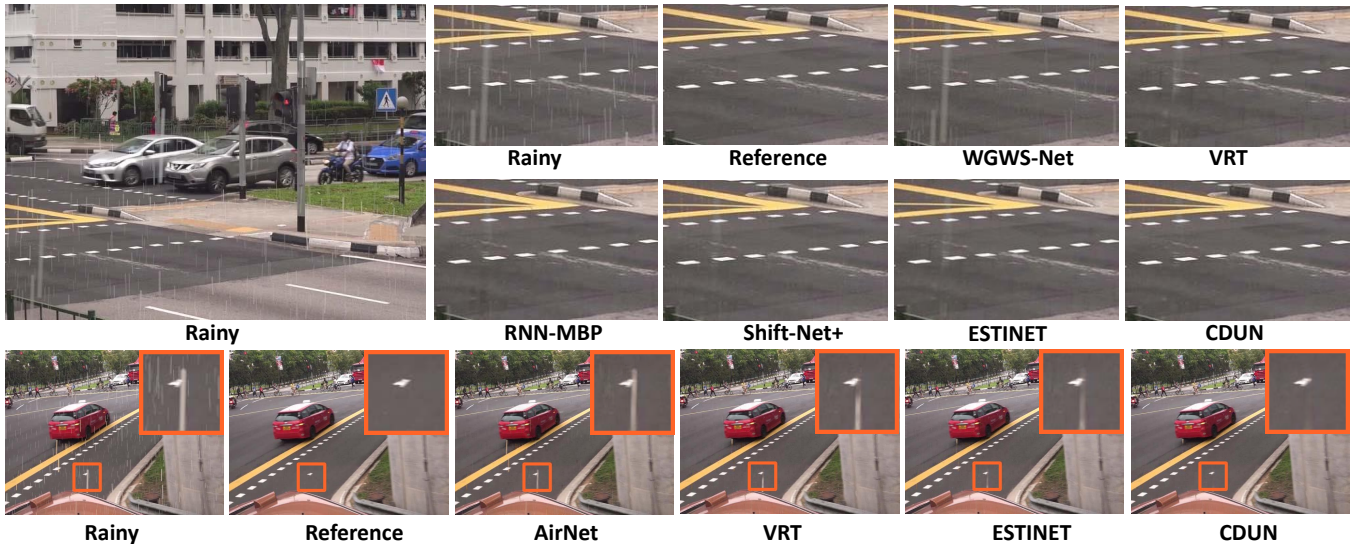


Fig. 7. Visual comparison of video rain removal results on the NTURain dataset [62] among different methods. The proposed CDUN restores a cleaner background frame compared to other methods.

To facilitate practical implementation, we calculate $U_{i \rightarrow j}$ (as defined in Eq. 8) rather than directly computing $W_{i \rightarrow j}$ in practice. Specifically, we have:

$$\begin{aligned} U_{i \rightarrow j} &= M_{j \rightarrow i}(W_{i \rightarrow j}^2) \\ &= M_{j \rightarrow i}f^2[M_{i \rightarrow j}(\|m_{i \rightarrow j}\|^2)]. \end{aligned} \quad (21)$$

Since f is a trainable network, the above equation is equivalent to:

$$M_{j \rightarrow i}\mathcal{F}[M_{i \rightarrow j}(\|m_{i \rightarrow j}\|^2)], \quad (22)$$

where \mathcal{F} is a trainable network. In practice, the structure of \mathcal{F} is defined as *convolution* \rightarrow *normalization* \rightarrow *ReLU* \rightarrow *convolution* \rightarrow *Sigmoid*. Due to the fact that \mathcal{F} does not have any positional impact on the elements in the matrix and is trainable, we can merge $M_{j \rightarrow i}$ and $M_{i \rightarrow j}$ as follows:

$$\begin{aligned} U_{i \rightarrow j} &= M_{j \rightarrow i}\{\mathcal{F}[M_{i \rightarrow j}(\|m_{i \rightarrow j}\|^2)]\} \\ &= \mathcal{F}\{M_{j \rightarrow i}[M_{i \rightarrow j}(\|m_{i \rightarrow j}\|^2)]\} \\ &= \mathcal{F}(\|m_{i \rightarrow j}\|^2). \end{aligned} \quad (23)$$

By employing the aforementioned simplification, we only need to calculate $U_{i \rightarrow j}^{(k-1)}$ using Eq. 23 (here, the superscript $k-1$ representing the iteration step is omitted) in practice.

IV. EXPERIMENTS AND ANALYSIS

In this section, we conducted experimental validations of the proposed method. Firstly, we described the experimental settings, followed by comparisons with existing state-of-the-art methods on both All-In-One VR and Task-Specific VR. Finally, we performed relevant ablation studies to demonstrate the effectiveness of the proposed key modules.

A. Experiment settings

Datasets. We validated the video restoration performance on four tasks: rain removal, haze removal, snow removal, and low-light enhancement (LLE). The detailed information of the training and testing datasets is presented in Tab. I. Due to the

lack of publicly available paired datasets of snow videos and clean videos, we utilized the DAVIS (2017 challenge, 480p) video dataset [63] and Adobe After Effects to synthesize snow videos and construct a paired dataset. The training set used in the All-In-One image restoration experiments is a combination of the four individual training sets.

TABLE I

THE DETAILED INFORMATION ABOUT THE DATASETS USED IN THIS WORK.

Task	Dataset	Number of Training Videos / Frames	Number of Testing Videos / Frames
Rain Removal	NTURain [62]	25/3.1k	8/1.7k
Haze Removal	REVIDE [64]	42/1.7k	6/0.3k
Snow Removal	DAVIS-snow [63]	90/6.2k	30/2.1k
LLE	SDSD [65]	125/32.1k	25/5.4k

Training. The training process in this work includes two stages: training of SADE and training of CDUN. Both stages utilize the same training datasets. During the data sampling process from the training dataset, we randomly select a contiguous sequence of frames with a length of l from the four degradation types with equal probability. For training SADE, the value of l is set to 7, while for training CDUN, l is set to 3. Simultaneously, the spatial scale of the training frame sequences is randomly cropped to a size of 256×256 , and data augmentation is performed by applying random horizontal flipping. In both training stages, we utilize the AdamW optimizer with a batch size of 4 and an initial learning rate of $2e-4$. The learning rate is reduced by a factor of one-tenth every $40k$ iterations, and a total of $100k$ iterations are performed.

Evaluation. We employ SSIM (Structural Similarity Index) [53] and PSNR (Peak Signal-to-Noise Ratio) as evaluation metrics to assess the video restoration quality. Additionally, we evaluate the computational cost of video restoration methods based on FLOPs (Floating-Point Operations), parameter quantity, and runtime. The FLOPs and runtime presented in

TABLE II
 QUANTITATIVE COMPARISON WITH STATE-OF-THE-ART METHODS ON ALL-IN-ONE VR. IN THE TABLE, THE BEST SCORE IS HIGHLIGHTED IN **BOLD** AND THE SECOND-BEST SCORE IS UNDERLINED.

	Type	All-In-One IR Method				Task-Specific VR Method						All-In-One VR Method
	Method	TransWeather [66]	Chen <i>et al.</i> [14]	AirNet [13]	WGWS-Net [16]	STFAN [67]	SDSD [65]	VRT [32]	RNN-MBP [8]	ESTINET [68]	Shift-Net+ [61]	CDUN (Ours)
Rain Removal	PSNR \uparrow	30.16	31.79	31.82	32.07	31.25	32.79	34.25	34.32	<u>35.49</u>	34.99	37.16 (+1.67)
	SSIM \uparrow	0.923	0.936	0.941	0.945	0.936	0.946	0.952	0.951	<u>0.956</u>	0.953	0.969 (+0.013)
Hazy Removal	PSNR \uparrow	18.27	21.12	21.21	21.93	19.76	21.99	22.34	22.21	22.52	<u>22.63</u>	23.54 (+0.91)
	SSIM \uparrow	0.837	0.855	0.860	0.868	0.843	0.867	0.886	0.881	0.888	<u>0.890</u>	0.899 (+0.009)
Snow Removal	PSNR \uparrow	28.96	29.73	30.32	30.57	29.24	29.72	31.17	31.30	31.46	<u>31.82</u>	33.78 (+1.96)
	SSIM \uparrow	0.881	0.895	0.905	0.911	0.886	0.892	0.913	0.912	0.917	<u>0.925</u>	0.942 (+0.017)
LLE	PSNR \uparrow	20.17	21.61	22.03	22.05	21.10	23.12	23.18	23.26	23.28	<u>23.31</u>	24.18 (+0.87)
	SSIM \uparrow	0.628	0.633	0.636	0.642	0.625	0.654	0.655	0.660	0.663	<u>0.676</u>	0.694 (+0.018)
Average	PSNR \uparrow	24.39	26.06	26.34	26.65	25.34	26.91	27.73	27.77	<u>28.19</u>	<u>28.19</u>	29.67 (+1.48)
	SSIM \uparrow	0.817	0.830	0.836	0.842	0.823	0.840	0.852	0.851	0.856	<u>0.861</u>	0.876 (+0.015)

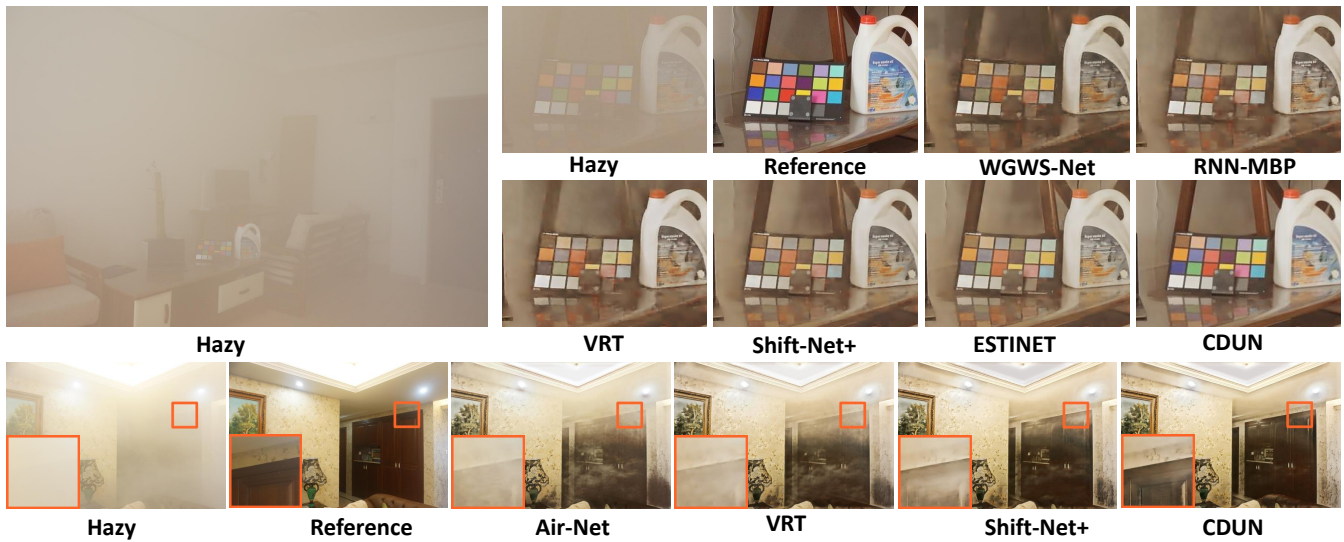


Fig. 8. Visual comparison of video haze removal results on the REVIDE dataset [64] among different methods. The proposed CDUN can capture degradation features such as haze density, resulting in fewer artifacts in the restored output.

the tables of this paper represent the average computation and runtime per frame. \uparrow in the table indicates that the higher the score, the better the performance.

B. Comparisons on All-In-One Video Restoration

In this work, we compared the proposed CDUN with existing state-of-the-art methods on the All-In-One VR task. Tab II presents the scores of different methods on multiple datasets. As this study is the first investigation into All-In-One VR, we compared it with some excellent existing All-In-One IR and Task-Specific VR methods. As shown in Table 1, the proposed method outperforms other methods on all four tasks. Specifically, compared to the second-best method, the proposed approach achieves an average PSNR improvement of 1.48dB and an SSIM improvement of 0.015.

Furthermore, illustrated in Fig. 7, 8, 9, and 10, we present qualitative comparisons of the proposed CDUN with existing

methods on video rain removal, haze removal, snow removal, and low-light enhancement tasks. It is evident that, the videos restored by CDUN exhibit more visually pleasing results compared to other methods.

The proposed CDUN has been validated through quantitative and qualitative comparisons, demonstrating its significant advantages over existing methods in All-In-One VR. Additionally, we visualized the degradation matrices estimated by SADE in the All-In-One VR task, and they are presented in Fig. 4. Indeed, the degradation matrices model different degradation features, such as rain streaks, haze density, snowflake, and lighting intensity. The proposed CDUN achieves adaptive removal of different types of degradations through guidance from different degradation matrices.

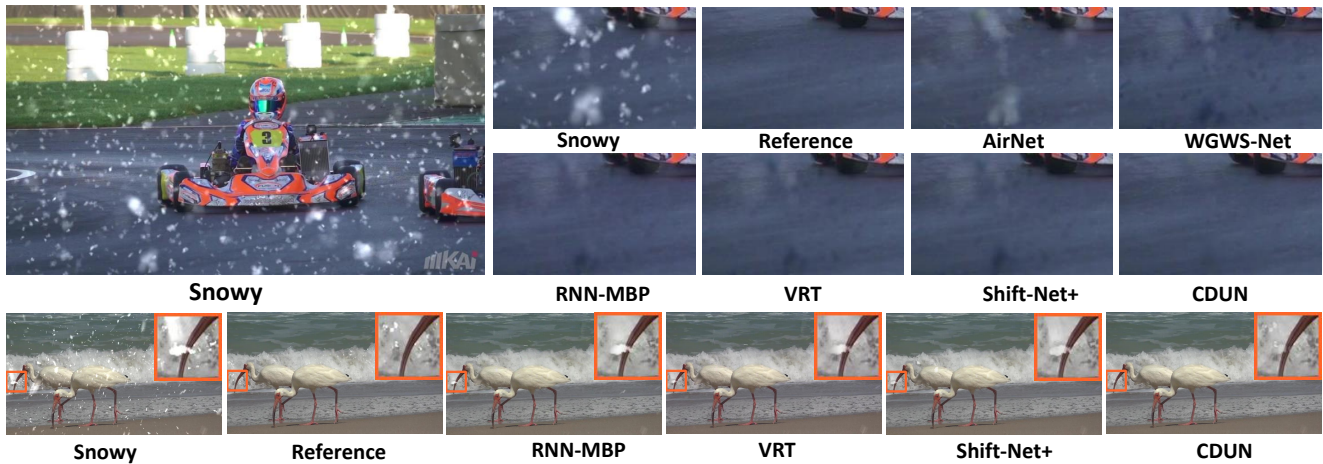


Fig. 9. Visual comparison of video snow removal results on the DAVIS-snow dataset [63] among different methods. It can be seen from the figure that the proposed CDUN achieves outstanding results in removing large snowflakes.

TABLE III
 QUANTITATIVE COMPARISON WITH STATE-OF-THE-ART METHODS ON TASK-SPECIFIC VR. IN THE TABLE, THE BEST SCORE IS HIGHLIGHTED IN **BOLD** AND THE SECOND-BEST SCORE IS UNDERLINED.

Task	Method	MS-CSC [69]	JORDER [70]	FastDerain [71]	J4RNet [72]	SPAC [62]	FCRNet [73]	SLDNet+ [74]	ESTINET [68]	CDUN
		Rain Removal	PSNR	27.31	32.61	30.32	32.14	33.11	36.05	<u>38.36</u>
	SSIM	0.7870	0.9482	0.9262	0.9480	0.9474	0.9676	<u>0.9750</u>	0.9700	0.9760
Haze Removal	Method	MSBDN [75]	FFA [76]	VDH [77]	EDVR [24]	CG-IDN [64]	NCFL [78]	BasicVSR++ [79]	MAP-Net [80]	CDUN
	PSNR \uparrow	22.01	16.65	16.64	21.22	23.21	23.63	21.68	<u>24.16</u>	24.31
	SSIM \uparrow	0.8759	0.8133	0.8133	0.8707	0.8836	0.8925	0.8726	<u>0.9043</u>	0.9109
Snow Removal	Method	MS-CSC [69]	SPAC [62]	FCR-Net [73]	MAP-Net [80]	SLDNet+ [74]	RNN-MBP [8]	ESTINET [68]	Shift-Net+ [61]	CDUN
	PSNR \uparrow	29.07	29.90	30.39	31.77	32.60	33.24	33.14	<u>33.85</u>	34.73
	SSIM \uparrow	0.8874	0.9025	0.9081	0.9202	0.9293	0.9371	0.9408	<u>0.9447</u>	0.9613
LLE	Method	DeepUPE [81]	DeepLPF [82]	DRBN [83]	MBLLEN [84]	SMID [85]	SMOID [86]	StableLLVE [64]	SDSD [65]	CDUN
	PSNR \uparrow	21.91	22.14	22.23	21.48	23.74	23.17	23.41	<u>24.23</u>	24.58
	SSIM \uparrow	0.66	0.63	0.63	0.61	<u>0.69</u>	0.65	0.67	0.70	

C. Comparisons on Task-Specific Video Restoration

Since there are currently only task-Specific VR methods and this work is the first work about All-In-One VR, we also conducted Task-Specific VR experiments for direct comparisons with existing methods. Following the works of Zhang *et al.* [68], Xu *et al.* [80], Yang *et al.* [74] and Wang *et al.* [65], we trained the proposed method using the same experimental settings as theirs. Subsequently, we conducted quantitative comparisons on video rain removal, haze removal, snow removal, and low-light enhancement tasks. As shown in Tab. III, the proposed CDUN achieved the highest performance scores in all tasks. This is because the iterative process of CDUN expands the temporal receptive fields, enabling the fusion of more data from additional frames to aid video restoration. This mechanism is beneficial for both types (All-In-One and Task-Specific) of video restoration tasks.

D. Ablation Study

In this section, we conducted ablation studies blou key modules to explore their individual contributions and functionalities. All experiments are conducted on the All-In-One VR

task. The scores of the best-performing results are highlighted in **bold** in the tables.

The effect of SADE. Our proposed CDUN utilizes SADE to adaptively estimate the degradation matrices, thereby guiding the optimization process based on Eq. 4 to adaptively remove the corresponding type of degradation. SADE achieves the adaptive adjust of the network parameters based on the degradation characteristics present in the input video, enhancing the accuracy of degradation modeling in multi-degradation scenarios. Furthermore, the proposed SADE utilizes a sequence-wise dynamic mechanism instead of the classical frame-wise approach, effectively overcoming the instability issues associated with parameter generation in the latter. Due to the existing Task-Specific IR methods has directly used UFormer [38] to predict the degradation matrices [44], we conducted comparative experiments by replacing SADE with UFormer. As shown in the first row and the last row of Tab. IV, employing SADE leads to a significant improvement in PSNR. This demonstrates that, compared to the proposed SADE, the static model (UFormer) is limited in its capability to handle multi-degradation scenarios effectively.



Fig. 10. Visual comparison of video low-light enhancement results on the SDDS dataset [65] among different methods. The proposed CDUN achieves more visually pleasing results compared to existing methods.

TABLE IV

THE ABLATION STUDY ON SADE, RWM, AND SPATIAL MOTION WEIGHT. THE TABLE PRESENTS THE PERFORMANCE SCORES (PSNR) OF ALL-IN-ONE VR UNDER VARIOUS EXPERIMENTAL CONFIGURATIONS.

SADE	RWM	Spatial Motion Weight	Rain Removal	Haze Removal	Snow Removal	LLE	Average
	✓	✓	35.27	22.64	32.92	22.30	28.28
✓		✓	32.26	20.07	27.96	20.76	25.26
✓	✓		36.85	23.08	31.99	22.66	28.65
✓	✓	✓	37.46	23.54	33.78	24.18	29.74

TABLE V

ABLATION STUDY ON SEQUENCE-WISE DYNAMIC AND FRAME-WISE DYNAMIC. THE TABLE PRESENTS A COMPARISON OF VR PERFORMANCE UNDER DIFFERENT EXPERIMENTAL SETTINGS, BASED ON PSNR SCORES.

Method	Rain Removal	Haze Removal	Snow Removal	LLE	Average
Frame-wise	34.51	21.61	32.09	23.06	27.82
Sequence-wise	37.46	23.54	33.78	24.18	29.74

Advantages of Sequence-wise dynamics over frame-wise dynamics. This work introduces a SADE for adaptive estimating various types of degradation matrices. The conventional Frame-wise approach involves generating dynamic parameters

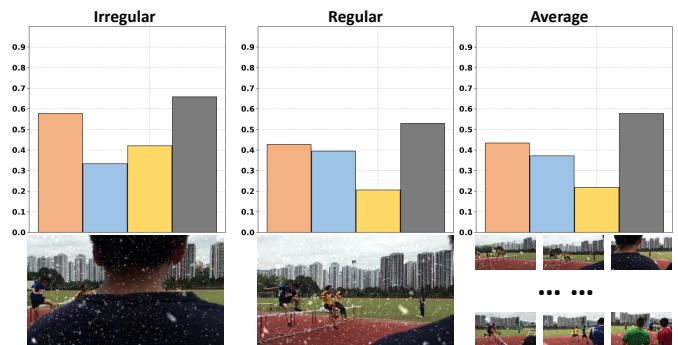


Fig. 11. The visualization of expert weights in SADE under the Frame-wise strategy. The bar chart displays the values of the four expert weights. In the Frame-wise setting, when the background information differs significantly from other frames (as seen in the leftmost column), there are considerable variations in expert weights. This background sensitivity hinders the adaptive estimation of the degradation matrices.

based on the features of each frame to process that particular frame. However, this is not suitable for estimating degradation matrices in All-In-One VR. As shown in Fig. 11, we trained the SADE using the Frame-wise architecture and visualized the expert weights (denoted as w_i in Eq. 15 and Fig. 5). To obtain a reference, we calculated the average of the weights from multiple frames, as shown in the third column of Fig. 11. We observed that when the background scene of individual frames significantly differs from that of the majority of frames (the first column of Fig. 11), the generated expert weights

TABLE VI

SADE GENERATES DYNAMIC PARAMETERS BY OBSERVING INFORMATION FROM m FRAMES. THE TABLE BELOW SHOWCASES THE PSNR SCORES AND FLOPs FOR DIFFERENT VALUES OF m .

m	Rain Removal	Haze Removal	Snow Removal	LLE	Average	FLOPs (G)
1	33.79	22.34	30.68	22.14	27.24	2.153
2	34.45	22.46	31.90	23.07	27.97	2.448
3	36.34	23.22	33.29	23.43	29.07	2.965
5	37.46	23.54	33.78	24.18	29.74	3.953

deviate significantly from the reference values as well. Our objective is to enable SADE to utilize different parameters for various degradation types, but the parameter adjustment in the frame-wise architecture is highly sensitive to background information. In this background-sensitive scenario, the model tends to waste its representation capacity on processing the background, leading to a decrease in the estimation accuracy of the degradation matrices.

To address the aforementioned issues, we propose the Sequence-wise dynamic strategy, which involves generating dynamic parameters by observing multiple frames within a video segment and sharing these parameters while processing individual frames within that video. Typically, degradation within a video segment is of the same type. Therefore, the introduced Sequence-wise dynamic strategy overcomes the limitations of the Frame-wise approach without compromising the model’s dynamic nature. Tab. V presents a quantitative comparison between the two strategies. Additionally, we conducted an ablation study on the number of frames (m) used for parameter generation, and the relevant experimental results are provided in Tab. VI. The final SADE model generates dynamic parameters by observing five frames, uniformly sampled at equal intervals.

The effect of RWM. The proposed CDUN requires explicit alignment, but existing explicit alignment methods often suffer from decreased accuracy due to the influence of long displacements and motion blur. Therefore, we introduce the RMW module to improve alignment precision while maintaining the explicit alignment paradigm. From Fig. 6, it can be observed that due to the presence of errors in optical flow estimation, direct alignment based on optical flow may result in structural distortions. To address this issue, we introduced a corrective step after the explicit warping operation. This step involves extracting structural information from the target matrix (see Sec. III-F for details) to rectify the results, aiming to mitigate the adverse effects of optical flow inaccuracies and reduce structural distortions in the aligned output. The experimental results in row 2 and 4 of Tab. IV reveal that the proposed RMW (Residual Motion Warping) module plays a crucial role.

The effect of Spatial Motion Weight. Generally, during the process of video alignment, pixels that are displaced over longer distances tend to have larger optical flow errors. As a result, the reference value for frame restoration varies for pixels with different displacement distances. In this work, we address this issue by assigning different weights to pixels

with varying displacement distances, thereby enhancing the model’s tolerance toward the errors of optical flow estimating. As evident from the comparison between rows 2 and 4 in Tab. IV, it can be observed that the proposed Spatial Motion Weight play a crucial role in the overall performance.

TABLE VII

THE PERFORMANCE SCORES (PSNR AND SSIM) AND COMPUTATIONAL COST (FLOPs, PARAMETER QUANTITY, AND RUNTIME) ARE QUANTITATIVELY COMPARED IN DIFFERENT NUMBERS OF ITERATION STEPS. THE *avg* REPRESENTS THE AVERAGE SCORE ACROSS THE FOUR TASKS: RAIN REMOVAL, HAZE REMOVAL, SNOW REMOVAL, AND LOW-LIGHT ENHANCEMENT.

N	PSNR(<i>avg</i>)	SSIM(<i>avg</i>)	FLOPs (G)	#Params (M)	Runtime (s)
1	26.52	0.823	19.74	4.96	0.108
2	28.06	0.847	33.61	5.85	0.209
3	29.24	0.865	47.49	6.74	0.302
4	29.62	0.871	61.36	7.64	0.395
5	29.74	0.876	75.23	8.53	0.490

Number of iterations. The proposed CDUN performs All-In-One VR by iteratively optimizing Eq. 4 for a fixed number of steps. To determine the appropriate value of the iteration steps N , we conducted experiments to find the optimal value for N . As shown in Tab. VII, with an increase in the number of iteration steps, the PSNR, FLOPs, and parameter quantity of CDUN gradually increase. From Fig. 12, it can be observed that the acceleration of PSNR improvement decreases progressively, while the growth in computational cost follows a linear trend with a almost constant acceleration. This reflects that in later stages, further increasing the number of iteration steps has a lower cost-effectiveness in terms of performance improvement. Therefore, after considering the trade-off between computational cost and model performance, we ultimately chose to set the number of iteration steps to 5. Additionally, the temporal window length for each iteration step is set to 3. Consequently, for five iteration steps, the total temporal receptive field length can be calculated as $3 + (5 - 1) \times (3 - 1) = 11$. Such a temporal receptive field length is relatively sufficient for video restoration.

V. DISCUSSION

A. Study on the Expansion of Temporal Receptive Field and Its Impact

In this experiment, we validate that the proposed CDUN enlarges the temporal receptive field by stacking temporal windows during the iterative process. The experiment is conducted using the middle 13 frames of each video segment from the NTURain [62] dataset and DAVIS-snow [63] dataset. We number the middle frame as i and subsequently labeled the 13 frames as $i-6, i-5, \dots, i, \dots, i+5, i+6$. Theoretically, a temporal window with a length of $a = 3$ is stacked in each iteration. After $N = 5$ iterations, the size of the temporal window should be $a + (N - 1) \times (a - 1) = 11$. when we replace the $(i + j)$ -th frame with ground-truth, if the $(i + j)$ -th frame falls within the receptive field, the restoration of the i -th frame will benefit from the information obtained from that ground-truth frame.

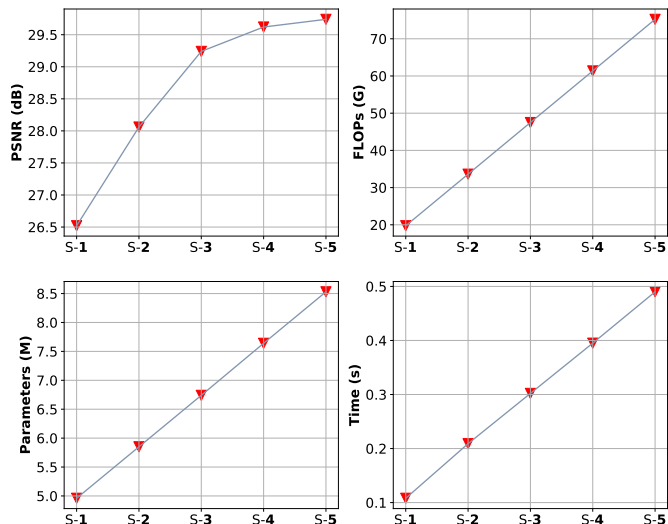


Fig. 12. The performance scores (PSNR and SSIM) and computational cost (FLOPs, parameter quantity, and runtime) are qualitatively compared in different numbers of iteration steps.

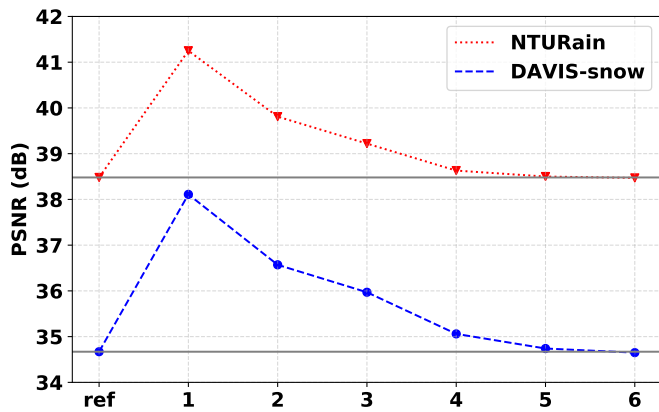


Fig. 13. In this experiment, we explore the temporal receptive field length by replacing adjacent frames with ground-truth frames and observing the performance score improvements. Here, *ref* represents the PSNR score without inserting ground-truth frames. The remaining horizontal coordinates represent the insertion position, denoted by the value of *j*.

Fig. 13 displays the average restoration scores of video segments from two datasets when inserting ground-truth frames at different positions. It can be observed that when *j* takes values from 1 to 5, the PSNR scores of the *i*-th frame all increase. This finding clearly demonstrates that CDUN can effectively leverage information from frames as far as *i* + 5. This observation is consistent with the theoretical temporal receptive field length (from the *i*-5 frame to the *i*+5 frame). It should be noted that dense degradations, such as haze and low-light conditions, result in significant discrepancies between the ground-truth and original frame pixel values. This discrepancy can severely interfere with optical flow estimation, consequently impacting the experimental results. Consequently, this experiment is only conducted on sparse degradations, namely rain and snow.

B. Relationship Between Image Restoration and Video Restoration.

In the framework of CDUN, All-In-One IR is a trivial form of All-In-One VR. In reference to Eq. 4, when the temporal window \mathcal{I} has a length of 1, *j* is equal to *i*. In this situation, the motion operator $M_{i \rightarrow i}$ becomes an identity mapping, and all pixels have a motion distance of 0. As a result, all components of the Spatial Motion Weights matrix $W_{i \rightarrow i}$ are equal. Therefore, we can omit $M_{i \rightarrow i}$, $W_{i \rightarrow i}$ and subscripts representing the frame indices in the video, and rewriting Eq. 4 as follows:

$$\hat{B} = \arg \min_B \frac{1}{2} \|F - (B \cdot T + D)\|^2 + \lambda \Phi(B). \quad (24)$$

Its corresponding MAP (Maximum a Posteriori) framework can be represented as follows:

$$\begin{aligned} \hat{B} &= \arg \max_B \log P(B|F) \\ &= \arg \max_B \log P(F|B) + \log P(B). \end{aligned} \quad (25)$$

The aforementioned optimization problem is a image restoration process [17]–[19], [44] with a degradation modeled as $F = TB + D$. When *T* and *D* are adaptively estimated, it constitutes an All-In-One image restoration process [49].

VI. CONCLUSION

In this paper, we propose for the first time an All-In-One VR method called Cross-Consistent Deep Unfolding Network (CDUN), which enables the restoration of different degraded videos with a single model. Specifically, CDUN consists of two core modules: (1) a well-designed SADE that can adaptively estimate the degradation matrices of differently degraded videos; and (2) a novel iterative optimization framework that can remove the degradation defined in the degradation matrices, from corrupted videos. By cascading the above two modules, CDUN achieves adaptive removal of diverse degradations. In addition, CDUN can capture complementary background information in adjacent frames by modeling inter-frame correlations within a temporal window, and can further expand the temporal receptive field by stacking windows. This mechanism enables the restoration of each frame to utilize the abundant features in long temporal-range frames. Consequently, by adaptive degradation removal and long-range feature utilization, the proposed CDUN is capable of effectively restoring videos corrupted by diverse degradations. Extensive experiments demonstrate that the proposed method achieves state-of-the-art performance in All-In-One VR.

VII. LIMITATION

The proposed method is based on a generalized degradation model, represented by Eq. 1. Therefore, the proposed CDUN is suitable for degradation types that conform to Eq. 1. However, for degradation types that do not comply with Eq. 1, the CDUN may not be applicable. For example, motion blur is typically modeled as the convolution of a clean background with a blur kernel [20], [87], rather than being represented by a multiplicative and an additive factor as in Eq. 1.

REFERENCES

- [1] N. Carion, F. Massa, G. Synnaeve, N. Usunier, A. Kirillov, and S. Zagoruyko, "End-to-end object detection with transformers," in *European conference on computer vision*. Springer, 2020, pp. 213–229.
- [2] C.-Y. Wang, A. Bochkovskiy, and H.-Y. M. Liao, "Yolov7: Trainable bag-of-freebies sets new state-of-the-art for real-time object detectors," in *Proceedings of the IEEE/CVF Conference on Computer Vision and Pattern Recognition*, 2023, pp. 7464–7475.
- [3] L.-C. Chen, Y. Zhu, G. Papandreou, F. Schroff, and H. Adam, "Encoder-decoder with atrous separable convolution for semantic image segmentation," in *Proceedings of the European conference on computer vision (ECCV)*, 2018, pp. 801–818.
- [4] Q. Yu, H. Wang, S. Qiao, M. Collins, Y. Zhu, H. Adam, A. Yuille, and L.-C. Chen, "k-means mask transformer," in *European Conference on Computer Vision*. Springer, 2022, pp. 288–307.
- [5] T. Xue, B. Chen, J. Wu, D. Wei, and W. T. Freeman, "Video enhancement with task-oriented flow," *International Journal of Computer Vision*, vol. 127, pp. 1106–1125, 2019.
- [6] Y. Tian, Y. Zhang, Y. Fu, and C. X. Tdan, "temporally-deformable alignment network for video super-resolution. in 2020 ieee," in *CVF Conference on Computer Vision and Pattern Recognition (CVPR)*, 2020, pp. 3357–3366.
- [7] K. C. Chan, X. Wang, K. Yu, C. Dong, and C. C. Loy, "Understanding deformable alignment in video super-resolution," in *Proceedings of the AAAI conference on artificial intelligence*, vol. 35, no. 2, 2021, pp. 973–981.
- [8] C. Zhu, H. Dong, J. Pan, B. Liang, Y. Huang, L. Fu, and F. Wang, "Deep recurrent neural network with multi-scale bi-directional propagation for video deblurring," in *Proceedings of the AAAI conference on artificial intelligence*, vol. 36, no. 3, 2022, pp. 3598–3607.
- [9] Z. Xia, F. Perazzi, M. Gharbi, K. Sunkavalli, and A. Chakrabarti, "Basis prediction networks for effective burst denoising with large kernels," in *Proceedings of the IEEE/CVF Conference on Computer Vision and Pattern Recognition*, 2020, pp. 11 844–11 853.
- [10] A. Dosovitskiy, P. Fischer, E. Ilg, P. Hausser, C. Hazirbas, V. Golkov, P. Van Der Smagt, D. Cremers, and T. Brox, "FlowNet: Learning optical flow with convolutional networks," in *Proceedings of the IEEE international conference on computer vision*, 2015, pp. 2758–2766.
- [11] J. Dai, H. Qi, Y. Xiong, Y. Li, G. Zhang, H. Hu, and Y. Wei, "Deformable convolutional networks," in *Proceedings of the IEEE international conference on computer vision*, 2017, pp. 764–773.
- [12] R. Li, R. T. Tan, and L.-F. Cheong, "All in one bad weather removal using architectural search," in *Proceedings of the IEEE/CVF conference on computer vision and pattern recognition*, 2020, pp. 3175–3185.
- [13] B. Li, X. Liu, P. Hu, Z. Wu, J. Lv, and X. Peng, "All-in-one image restoration for unknown corruption," in *Proceedings of the IEEE/CVF Conference on Computer Vision and Pattern Recognition*, 2022, pp. 17 452–17 462.
- [14] W.-T. Chen, Z.-K. Huang, C.-C. Tsai, H.-H. Yang, J.-J. Ding, and S.-Y. Kuo, "Learning multiple adverse weather removal via two-stage knowledge learning and multi-contrastive regularization: Toward a unified model," in *Proceedings of the IEEE/CVF Conference on Computer Vision and Pattern Recognition*, 2022, pp. 17 653–17 662.
- [15] D. Park, B. H. Lee, and S. Y. Chun, "All-in-one image restoration for unknown degradations using adaptive discriminative filters for specific degradations," in *Proceedings of the IEEE/CVF Conference on Computer Vision and Pattern Recognition*, 2023, pp. 5815–5824.
- [16] Y. Zhu, T. Wang, X. Fu, X. Yang, X. Guo, J. Dai, Y. Qiao, and X. Hu, "Learning weather-general and weather-specific features for image restoration under multiple adverse weather conditions," in *Proceedings of the IEEE/CVF Conference on Computer Vision and Pattern Recognition*, 2023, pp. 21 747–21 758.
- [17] K. Zhang, W. Zuo, S. Gu, and L. Zhang, "Learning deep cnn denoiser prior for image restoration," in *Proceedings of the IEEE conference on computer vision and pattern recognition*, 2017, pp. 3929–3938.
- [18] C. Mou, Q. Wang, and J. Zhang, "Deep generalized unfolding networks for image restoration," in *Proceedings of the IEEE/CVF Conference on Computer Vision and Pattern Recognition*, 2022, pp. 17 399–17 410.
- [19] W. Wu, J. Weng, P. Zhang, X. Wang, W. Yang, and J. Jiang, "Uretinex-net: Retinex-based deep unfolding network for low-light image enhancement," in *Proceedings of the IEEE/CVF conference on computer vision and pattern recognition*, 2022, pp. 5901–5910.
- [20] K. Zhang, L. V. Gool, and R. Timofte, "Deep unfolding network for image super-resolution," in *Proceedings of the IEEE/CVF conference on computer vision and pattern recognition*, 2020, pp. 3217–3226.
- [21] L. Sun, Y. Wang, F. Wu, X. Li, W. Dong, and G. Shi, "Deep unfolding network for efficient mixed video noise removal," *IEEE Transactions on Circuits and Systems for Video Technology*, 2023.
- [22] X. Shi, Z. Huang, W. Bian, D. Li, M. Zhang, K. C. Cheung, S. See, H. Qin, J. Dai, and H. Li, "Videoflow: Exploiting temporal cues for multi-frame optical flow estimation," *arXiv preprint arXiv:2303.08340*, 2023.
- [23] J. Pan, H. Bai, and J. Tang, "Cascaded deep video deblurring using temporal sharpness prior," in *Proceedings of the IEEE/CVF conference on computer vision and pattern recognition*, 2020, pp. 3043–3051.
- [24] X. Wang, K. C. Chan, K. Yu, C. Dong, and C. Change Loy, "Edvr: Video restoration with enhanced deformable convolutional networks," in *Proceedings of the IEEE/CVF conference on computer vision and pattern recognition workshops*, 2019, pp. 0–0.
- [25] D. Li, C. Xu, K. Zhang, X. Yu, Y. Zhong, W. Ren, H. Suominen, and H. Li, "Arvo: Learning all-range volumetric correspondence for video deblurring," in *Proceedings of the IEEE/CVF Conference on Computer Vision and Pattern Recognition*, 2021, pp. 7721–7731.
- [26] H. Son, J. Lee, J. Lee, S. Cho, and S. Lee, "Recurrent video deblurring with blur-invariant motion estimation and pixel volumes," *ACM Transactions on Graphics (TOG)*, vol. 40, no. 5, pp. 1–18, 2021.
- [27] T. Isobe, S. Li, X. Jia, S. Yuan, G. Slabaugh, C. Xu, Y.-L. Li, S. Wang, and Q. Tian, "Video super-resolution with temporal group attention," in *Proceedings of the IEEE/CVF conference on computer vision and pattern recognition*, 2020, pp. 8008–8017.
- [28] W. Li, X. Tao, T. Guo, L. Qi, J. Lu, and J. Jia, "Mucan: Multi-correspondence aggregation network for video super-resolution," in *Computer Vision—ECCV 2020: 16th European Conference, Glasgow, UK, August 23–28, 2020, Proceedings, Part X 16*. Springer, 2020, pp. 335–351.
- [29] K. C. Chan, X. Wang, K. Yu, C. Dong, and C. C. Loy, "Basicvsr: The search for essential components in video super-resolution and beyond," in *Proceedings of the IEEE/CVF conference on computer vision and pattern recognition*, 2021, pp. 4947–4956.
- [30] T. Isobe, F. Zhu, X. Jia, and S. Wang, "Revisiting temporal modeling for video super-resolution," *arXiv preprint arXiv:2008.05765*, 2020.
- [31] S. Nah, S. Son, and K. M. Lee, "Recurrent neural networks with intra-frame iterations for video deblurring," in *Proceedings of the IEEE/CVF conference on computer vision and pattern recognition*, 2019, pp. 8102–8111.
- [32] J. Liang, J. Cao, Y. Fan, K. Zhang, R. Ranjan, Y. Li, R. Timofte, and L. Van Gool, "Vrt: A video restoration transformer," *arXiv preprint arXiv:2201.12288*, 2022.
- [33] Y.-C. Wan, M.-W. Shao, Y.-S. Cheng, Y.-X. Liu, Z.-Y. Bao, and D.-Y. Meng, "Restoring images captured in arbitrary hybrid adverse weather conditions in one go," *arXiv preprint arXiv:2305.09996*, 2023.
- [34] J. Zhang, J. Huang, M. Yao, Z. Yang, H. Yu, M. Zhou, and F. Zhao, "Ingredient-oriented multi-degradation learning for image restoration," in *Proceedings of the IEEE/CVF Conference on Computer Vision and Pattern Recognition*, 2023, pp. 5825–5835.
- [35] Y. Cheng, M. Shao, Y. Wan, Y. Liu, H. Liu, and D. Meng, "Deep fuzzy clustering transformer: Learning the general property of corruptions for degradation-agnostic multi-task image restoration," *IEEE Transactions on Fuzzy Systems*, 2023.
- [36] S. W. Zamir, A. Arora, S. Khan, M. Hayat, F. S. Khan, M.-H. Yang, and L. Shao, "Multi-stage progressive image restoration," in *Proceedings of the IEEE/CVF conference on computer vision and pattern recognition*, 2021, pp. 14 821–14 831.
- [37] S. W. Zamir, A. Arora, S. Khan, M. Hayat, F. S. Khan, and M.-H. Yang, "Restormer: Efficient transformer for high-resolution image restoration," in *Proceedings of the IEEE/CVF conference on computer vision and pattern recognition*, 2022, pp. 5728–5739.
- [38] Z. Wang, X. Cun, J. Bao, W. Zhou, J. Liu, and H. Li, "Uformer: A general u-shaped transformer for image restoration," in *Proceedings of the IEEE/CVF conference on computer vision and pattern recognition*, 2022, pp. 17 683–17 693.
- [39] Y. Wan, Y. Cheng, M. Shao, and J. González, "Image rain removal and illumination enhancement done in one go," *Knowledge-Based Systems*, vol. 252, p. 109244, 2022.
- [40] D. Geman and C. Yang, "Nonlinear image recovery with half-quadratic regularization," *IEEE transactions on Image Processing*, vol. 4, no. 7, pp. 932–946, 1995.
- [41] S. Boyd, N. Parikh, E. Chu, B. Peleato, J. Eckstein *et al.*, "Distributed optimization and statistical learning via the alternating direction method of multipliers," *Foundations and Trends® in Machine Learning*, vol. 3, no. 1, pp. 1–122, 2011.

- [42] A. Barbu, "Training an active random field for real-time image denoising," *IEEE Transactions on Image Processing*, vol. 18, no. 11, pp. 2451–2462, 2009.
- [43] K. G. Samuel and M. F. Tappen, "Learning optimized map estimates in continuously-valued mrf models," in *2009 IEEE Conference on Computer Vision and Pattern Recognition*. IEEE, 2009, pp. 477–484.
- [44] L. Guo, C. Wang, W. Yang, S. Huang, Y. Wang, H. Pfister, and B. Wen, "Shadowdiffusion: When degradation prior meets diffusion model for shadow removal," in *Proceedings of the IEEE/CVF Conference on Computer Vision and Pattern Recognition*, 2023, pp. 14 049–14 058.
- [45] D.-A. Huang, L.-W. Kang, M.-C. Yang, C.-W. Lin, and Y.-C. F. Wang, "Context-aware single image rain removal," in *2012 IEEE International Conference on Multimedia and Expo*. IEEE, 2012, pp. 164–169.
- [46] K. He, J. Sun, and X. Tang, "Single image haze removal using dark channel prior," *IEEE transactions on pattern analysis and machine intelligence*, vol. 33, no. 12, pp. 2341–2353, 2010.
- [47] Y.-F. Liu, D.-W. Jaw, S.-C. Huang, and J.-N. Hwang, "Desnownet: Context-aware deep network for snow removal," *IEEE Transactions on Image Processing*, vol. 27, no. 6, pp. 3064–3073, 2018.
- [48] R. Liu, L. Ma, J. Zhang, X. Fan, and Z. Luo, "Retinex-inspired unrolling with cooperative prior architecture search for low-light image enhancement," in *Proceedings of the IEEE/CVF Conference on Computer Vision and Pattern Recognition*, 2021, pp. 10 561–10 570.
- [49] Y. Cheng, M. Shao, Y. Wan, C. Wang, and W. Zuo, "Drm-ir: Task-adaptive deep unfolding network for all-in-one image restoration," *arXiv preprint arXiv:2307.07688*, 2023.
- [50] K. Zhang, W. Zuo, Y. Chen, D. Meng, and L. Zhang, "Beyond a gaussian denoiser: Residual learning of deep cnn for image denoising," *IEEE transactions on image processing*, vol. 26, no. 7, pp. 3142–3155, 2017.
- [51] O. Ronneberger, P. Fischer, and T. Brox, "U-net: Convolutional networks for biomedical image segmentation," in *Medical Image Computing and Computer-Assisted Intervention—MICCAI 2015: 18th International Conference, Munich, Germany, October 5–9, 2015, Proceedings, Part III 18*. Springer, 2015, pp. 234–241.
- [52] L. Kong, C. Shen, and J. Yang, "FastflowNet: A lightweight network for fast optical flow estimation," in *2021 IEEE International Conference on Robotics and Automation (ICRA)*. IEEE, 2021, pp. 10 310–10 316.
- [53] L.-T. Wang, N. E. Hoover, E. H. Porter, and J. J. Zasio, "Ssim: A software leveled compiled-code simulator," in *Proceedings of the 24th ACM/IEEE Design Automation Conference*, 1987, pp. 2–8.
- [54] P. Charbonnier, L. Blanc-Feraud, G. Aubert, and M. Barlaud, "Two deterministic half-quadratic regularization algorithms for computed imaging," in *Proceedings of 1st international conference on image processing*, vol. 2. IEEE, 1994, pp. 168–172.
- [55] S. Shan, Y. Li, and J. B. Oliva, "Meta-neighborhoods," *Advances in Neural Information Processing Systems*, vol. 33, pp. 5047–5057, 2020.
- [56] M. Denil, B. Shakibi, L. Dinh, M. Ranzato, and N. De Freitas, "Predicting parameters in deep learning," *Advances in neural information processing systems*, vol. 26, 2013.
- [57] E. Park, D. Kim, S. Kim, Y.-D. Kim, G. Kim, S. Yoon, and S. Yoo, "Big/little deep neural network for ultra low power inference," in *2015 International Conference on Hardware/Software Codesign and System Synthesis (CODES+ ISSS)*. IEEE, 2015, pp. 124–132.
- [58] G. Huang, D. Chen, T. Li, F. Wu, L. Van Der Maaten, and K. Q. Weinberger, "Multi-scale dense networks for resource efficient image classification," *arXiv preprint arXiv:1703.09844*, 2017.
- [59] B. Yang, G. Bender, Q. V. Le, and J. Ngiam, "ConDconv: Conditionally parameterized convolutions for efficient inference," *Advances in neural information processing systems*, vol. 32, 2019.
- [60] A. Vaswani, N. Shazeer, N. Parmar, J. Uszkoreit, L. Jones, A. N. Gomez, Ł. Kaiser, and I. Polosukhin, "Attention is all you need," *Advances in neural information processing systems*, vol. 30, 2017.
- [61] D. Li, X. Shi, Y. Zhang, K. C. Cheung, S. See, X. Wang, H. Qin, and H. Li, "A simple baseline for video restoration with grouped spatial-temporal shift," in *Proceedings of the IEEE/CVF Conference on Computer Vision and Pattern Recognition*, 2023, pp. 9822–9832.
- [62] J. Chen, C.-H. Tan, J. Hou, L.-P. Chau, and H. Li, "Robust video content alignment and compensation for rain removal in a cnn framework," in *Proceedings of the IEEE conference on computer vision and pattern recognition*, 2018, pp. 6286–6295.
- [63] J. Pont-Tuset, F. Perazzi, S. Caelles, P. Arbeláez, A. Sorkine-Hornung, and L. Van Gool, "The 2017 davis challenge on video object segmentation," *arXiv preprint arXiv:1704.00675*, 2017.
- [64] X. Zhang, H. Dong, J. Pan, C. Zhu, Y. Tai, C. Wang, J. Li, F. Huang, and F. Wang, "Learning to restore hazy video: A new real-world dataset and a new method," in *Proceedings of the IEEE/CVF Conference on Computer Vision and Pattern Recognition*, 2021, pp. 9239–9248.
- [65] R. Wang, X. Xu, C.-W. Fu, J. Lu, B. Yu, and J. Jia, "Seeing dynamic scene in the dark: A high-quality video dataset with mechatronic alignment," in *Proceedings of the IEEE/CVF International Conference on Computer Vision*, 2021, pp. 9700–9709.
- [66] J. M. J. Valanarasu, R. Yasarla, and V. M. Patel, "Transweather: Transformer-based restoration of images degraded by adverse weather conditions," in *Proceedings of the IEEE/CVF Conference on Computer Vision and Pattern Recognition*, 2022, pp. 2353–2363.
- [67] S. Zhou, J. Zhang, J. Pan, H. Xie, W. Zuo, and J. Ren, "Spatio-temporal filter adaptive network for video deblurring," in *Proceedings of the IEEE/CVF international conference on computer vision*, 2019, pp. 2482–2491.
- [68] K. Zhang, D. Li, W. Luo, W. Ren, and W. Liu, "Enhanced spatio-temporal interaction learning for video deraining: faster and better," *IEEE Transactions on Pattern Analysis and Machine Intelligence*, vol. 45, no. 1, pp. 1287–1293, 2022.
- [69] M. Li, Q. Xie, Q. Zhao, W. Wei, S. Gu, J. Tao, and D. Meng, "Video rain streak removal by multiscale convolutional sparse coding," in *Proceedings of the IEEE conference on computer vision and pattern recognition*, 2018, pp. 6644–6653.
- [70] W. Yang, R. T. Tan, J. Feng, J. Liu, Z. Guo, and S. Yan, "Deep joint rain detection and removal from a single image," in *Proceedings of the IEEE conference on computer vision and pattern recognition*, 2017, pp. 1357–1366.
- [71] T.-X. Jiang, T.-Z. Huang, X.-L. Zhao, L.-J. Deng, and Y. Wang, "Fasterain: A novel video rain streak removal method using directional gradient priors," *IEEE Transactions on Image Processing*, vol. 28, no. 4, pp. 2089–2102, 2018.
- [72] J. Liu, W. Yang, S. Yang, and Z. Guo, "Erase or fill? deep joint recurrent rain removal and reconstruction in videos," in *Proceedings of the IEEE conference on computer vision and pattern recognition*, 2018, pp. 3233–3242.
- [73] W. Yang, J. Liu, and J. Feng, "Frame-consistent recurrent video deraining with dual-level flow," in *Proceedings of the IEEE/CVF conference on computer vision and pattern recognition*, 2019, pp. 1661–1670.
- [74] W. Yang, R. T. Tan, S. Wang, A. C. Kot, and J. Liu, "Learning to remove rain in video with self-supervision," *IEEE Transactions on Pattern Analysis and Machine Intelligence*, 2022.
- [75] H. Dong, J. Pan, L. Xiang, Z. Hu, X. Zhang, F. Wang, and M.-H. Yang, "Multi-scale boosted dehazing network with dense feature fusion," in *Proceedings of the IEEE/CVF conference on computer vision and pattern recognition*, 2020, pp. 2157–2167.
- [76] J. Luo, Q. Bu, L. Zhang, and J. Feng, "Global feature fusion attention network for single image dehazing," in *2021 IEEE International Conference on Multimedia & Expo Workshops (ICMEW)*. IEEE, 2021, pp. 1–6.
- [77] W. Ren, J. Zhang, X. Xu, L. Ma, X. Cao, G. Meng, and W. Liu, "Deep video dehazing with semantic segmentation," *IEEE transactions on image processing*, vol. 28, no. 4, pp. 1895–1908, 2018.
- [78] C. Huang, J. Li, B. Li, D. Liu, and Y. Lu, "Neural compression-based feature learning for video restoration," in *Proceedings of the IEEE/CVF Conference on Computer Vision and Pattern Recognition*, 2022, pp. 5872–5881.
- [79] K. C. Chan, S. Zhou, X. Xu, and C. C. Loy, "Basicvsr++: Improving video super-resolution with enhanced propagation and alignment," in *Proceedings of the IEEE/CVF conference on computer vision and pattern recognition*, 2022, pp. 5972–5981.
- [80] J. Xu, X. Hu, L. Zhu, Q. Dou, J. Dai, Y. Qiao, and P.-A. Heng, "Video dehazing via a multi-range temporal alignment network with physical prior," in *Proceedings of the IEEE/CVF Conference on Computer Vision and Pattern Recognition*, 2023, pp. 18 053–18 062.
- [81] R. Wang, Q. Zhang, C.-W. Fu, X. Shen, W.-S. Zheng, and J. Jia, "Underexposed photo enhancement using deep illumination estimation," in *Proceedings of the IEEE/CVF conference on computer vision and pattern recognition*, 2019, pp. 6849–6857.
- [82] S. Moran, P. Marza, S. McDonagh, S. Parisot, and G. Slabaugh, "DeepLpf: Deep local parametric filters for image enhancement," in *Proceedings of the IEEE/CVF conference on computer vision and pattern recognition*, 2020, pp. 12 826–12 835.
- [83] W. Yang, S. Wang, Y. Fang, Y. Wang, and J. Liu, "From fidelity to perceptual quality: A semi-supervised approach for low-light image enhancement," in *Proceedings of the IEEE/CVF conference on computer vision and pattern recognition*, 2020, pp. 3063–3072.
- [84] F. Lv, F. Lu, J. Wu, and C. Lim, "Mblen: Low-light image/video enhancement using cnns," in *BMVC*, vol. 220, no. 1, 2018, p. 4.

- [85] C. Chen, Q. Chen, M. N. Do, and V. Koltun, "Seeing motion in the dark," in *Proceedings of the IEEE/CVF International conference on computer vision*, 2019, pp. 3185–3194.
- [86] H. Jiang and Y. Zheng, "Learning to see moving objects in the dark," in *Proceedings of the IEEE/CVF International Conference on Computer Vision*, 2019, pp. 7324–7333.
- [87] L. Pan, R. Hartley, M. Liu, and Y. Dai, "Phase-only image based kernel estimation for single image blind deblurring," in *Proceedings of the IEEE/CVF Conference on Computer Vision and Pattern Recognition*, 2019, pp. 6034–6043.